Since January 2020 Elsevier has created a COVID-19 resource centre with free information in English and Mandarin on the novel coronavirus COVID-19. The COVID-19 resource centre is hosted on Elsevier Connect, the company's public news and information website.

Biophysical Chemistry 288 (2022) 106854

Contents lists available at ScienceDirect

Biophysical Chemistry

journal homepage: www.elsevier.com/locate/biophyschem

Molecular docking and machine learning affinity prediction of compounds identified upon softwood bark extraction to the main protease of the SARS-CoV-2 virus

Michal Jablonský [a,*], Marek Štekláč [b], Veronika Majová [a], Marián Gall [c,d], Ján Matúška [e], Michal Pitoňák [d,f], Lukáš Bučinský [e,*]

[a] Institute of Natural and Synthetic Polymers, Department of Wood, Pulp and Paper, Faculty of Chemical and Food Technology, Slovak University of Technology in Bratislava, Radlinského 9, Bratislava SK-812 37, Slovakia
[b] Institute of Physical Chemistry and Chemical Physics, Department of Physical Chemistry, Faculty of Chemical and Food Technology, Slovak University of Technology in Bratislava, Radlinského 9, Bratislava SK-812 37, Slovakia
[c] Institute of Information Engineering, Automation and Mathematics, Faculty of Chemical and Food Technology, Slovak University of Technology in Bratislava, Radlinského 9, SK-81237 Bratislava, Slovak Republic
[d] Computing Center, Centre of Operations of the Slovak Academy of Sciences, Dúbravská cesta c. 9, SK-84535 Bratislava, Slovak Republic
[e] Institute of Physical Chemistry and Chemical Physics, Department of Chemical Physics, Faculty of Chemical and Food Technology, Slovak University of Technology in Bratislava, Radlinského 9, Bratislava SK-812 37, Slovakia
[f] Department of Physical and Theoretical Chemistry, Faculty of Natural Sciences, Comenius University in Bratislava, Mlynská dolina, Ilkovičova 6, SK-84215 Bratislava, Slovak Republic

ARTICLE INFO

Keywords:
SARS-CoV-2
3CL^{pro}
Softwood bark
Molecular docking
Machine learning

ABSTRACT

Molecular docking of 234 unique compounds identified in the softwood bark (**W** set) is presented with a focus on their inhibition potential to the main protease of the SARS-CoV-2 virus 3CL^{pro} (6WQF). The docking results are compared with the docking results of 866 COVID19-related compounds (**S** set). Furthermore, machine learning (ML) prediction of docking scores of the **W** set is presented using the **S** set trained TensorFlow, XGBoost, and SchNetPack ML approaches. Docking scores are evaluated with the Autodock 4.2.6 software. Four compounds in the **W** set achieve a docking score below −13 kcal/mol, with (+)-lariciresinol 9′-p-coumarate (CID 11497085) achieving the best docking score (−15 kcal/mol) within the **W** and **S** sets. In addition, 50% of **W** set docking scores are found below −8 kcal/mol and 25% below −10 kcal/mol. Therefore, the compounds identified in the softwood bark, show potential for antiviral activity upon extraction or further derivatization. The **W** set molecular docking studies are validated by means of molecular dynamics (five best compounds). The solubility (Log *S*, ESOL) and druglikeness of the best docking compounds in **S** and **W** sets are compared to evaluate the pharmacological potential of compounds identified in softwood bark.

1. Introduction

The new coronavirus SARS-CoV-2, that belongs to the group of betacoronaviruses, is the cause of the severe respiratory syndrome dubbed COVID-19 [1,2]. The virus spreads predominantly via respiratory droplets and general symptoms of COVID-19 in infected patients are as follows: fever resembling common influenza, mucus production, dyspnea, headache, sore throat/pharyngalgia, diarrhea, etc. [3]. Eventually, COVID-19 can lead to life-threatening symptoms of extraordinarily lethal pneumonia [4,5]. Patients infected with SARS-CoV-2, both symptomatic and asymptomatic, are reported to display a higher occurrence of the virus in their nasal cavity than in their throat [3,6,7].

SARS-CoV-2 itself is a positive-sense single stranded RNA virus, whose genome encodes four structural proteins that are responsible for the virion shape (envelope protein), pathogenesis (nucleocapsid protein), virus's entry to host's cells (spike glycoprotein) and subsequent release of the virion particles (membrane protein). Furthermore, the genome encodes 16 non-structural proteins, including vital inhibitory targets such as the main protease M^{pro} (also known as 3CL^{pro} from 3-chymotrypsin-like protease), the papain-like protease PL^{pro}, the

* Corresponding authors.
E-mail addresses: michal.jablonsky@stuba.sk (M. Jablonský), lukas.bucinsky@stuba.sk (L. Bučinský).

https://doi.org/10.1016/j.bpc.2022.106854
Received 30 March 2022; Received in revised form 3 June 2022; Accepted 21 June 2022
Available online 26 June 2022

helicase, the RNA-dependent RNA polymerase RdRp, which all play a crucial role in the transcription and replication of the virus's RNA [8–12].

$3CL^{pro}$ is a highly conserved three-domain protease that consists of ca. 306 amino acids. The domains I (residues 8–101) and II (residues 102–184) form a beta-barrel secondary structure, while the domain III consists of alpha-helices (residues 201–303). The last two domains are connected by a long loop (residues 185–200). The catalytic dyad capable of hydrolyzing peptide bonds in enzymes, consisting of a nucleophilic Cys145 and a proton acceptor counterpart His41, is located in a gap between domains I and II [13]. These two residues are coupled with Thr25 to form the S2 subside of the substrate binding region. Together with the S1 subside, formed by residues His41, Phe140, Glu143, His163, Glu166, and His172, S2 can participate in hydrophobic and electrostatic interactions with the potential inhibitors. Furthermore, three additional shallow subsides S3-S5, comprised of His41, Met49, Met165, Glu166, and Gln189, are located nearby and offer additional modes of inhibitor-protease complex stabilization. The presence of residues that can tolerate different functionalities, its role in the replication of the virus, as well as structural similarity of $3CL^{pro}$ with other species of coronaviruses, make it a prospective inhibitory target for drug design and/or refurbishment [14–16].

World-wide research shows that extractives found in natural resources play an important protective role in the fight against viruses. In general, plants can produce metabolites which display inhibitory effects on enzymes, proteins, and virus propagation [17]. Plant immunity is a complex system able to detect and deactivate attacking pathogens with various tools [18]. These compounds are produced as a reaction to both biotic and abiotic influences. Other options are the secondary plant metabolites which are not considered vital for the life of plant cells. Several projects focused on measuring the bonding energy between plant-based metabolites and SARS-CoV-2 proteins. According to Azim et al. [3], all the metabolites could serve as medicines against COVID-19 and it is recommended that in vivo testing begins to confirm obtained results. Parvez et al. [19] studied five plant-based cures, namely azobechalcone, rifampin, isolophirachalcone, tetrandrine, and fangchinoline. Over 3600 unique ligand conformers of compounds from Iraqi medicinal plants were docked to the human Angiotensin Converting Enzyme-2 (ACE2) by Al-Shuhaib et al. [20] to study the inhibition potential of virus entry into human cells. Moreover, all the suggested medications display potential inhibitory effects on the main protease $3CL^{pro}$, the RNA-dependent RNA polymerase, and the spike glycoprotein. All results were obtained by virtual screening and point towards the fact that plant-based compounds could be promising in SARS group related disease treatments. Despite these results, more experiments will have to be conducted to confirm or disprove the efficiency of plant-based compounds and metabolites against COVID-19. Currently, it is very problematic to determine which of the aforementioned or previously untested substances could become the main components in the fight against SARS-CoV-2 [3,18,19,21,22].

More than 450 herbs-natural compounds displayed their antiviral activity against SARS-CoV-2 and similar viruses. Many displayed the ability to inhibit protein pathways of the coronavirus host and interfere in various phases of the viral life cycle, such as viral entry into a host cell, membrane fusion, transcription, translation and replication processes, viral assembly, and viral release [18]. Evidence proving the effects of these plants and natural compounds was obtained using the same or very similar methods to those utilized in conventional medical research. The plants and secondary metabolites offer a great potential in the fight against coronaviruses, especially SARS-CoV-2 [18]. This was explored in the work of da Silva Hage-Melim et al. [23], in which essential oils components have been evaluated by means of molecular docking against several SARS-CoV-2 units including the main protease. A similar approach was reported by Wu et al. [8] with respect to traditional Chinese medicine and natural products. Molecular docking became the standard approach to screen for possibly active substances for a further evaluation by means of more demanding molecular dynamics simulations or further in vitro tests in a targeted drug development. Molecular docking studies of large data sets of compounds were reported [13,24–27]. Nevertheless, even the molecular docking step is demanding when a quick tool for shrinking a database of thousands of compounds to a reasonable time is desirable [24,25,28]. This can be achieved by means of machine learning (ML) prediction of docking scores [24,25,28].

Polyphenols represent the most numerous and widespread group of natural substances in the world of plants. Waste from the processing of coniferous trees represents a huge potential in terms of recovering substances of high added value [29,30]. The work of Jablonsky et al. [29] focused the authors' attention on summarizing the properties of 237 metabolites identified from various literature sources. It compiles 25 cytotoxic, 26 antioxidant, 42 antibacterial, 22 anti-inflammatory, 5 antimutagenic, 5 pharmacokinetic, and 50 substances with inhibition activity found in conifer bark extracts.

Herein, we focus on the His41 – Cys145 catalytic dyad of SARS-CoV-2 $3CL^{pro}$ to evaluate the inhibition potential of compounds (metabolites) found in conifer bark extracts [29], denoted as the **W** set. The results are compared with the findings of 866 COVID-19 related compounds [31], denoted as the **S** set. In addition, solubility (Log *S*, ESOL) and druglikeness of best docking compounds in **S** and **W** sets are considered. Docking scores of five best compounds are further validated by means of molecular dynamics. Subsequently, the performance of ML docking scores prediction is evaluated according to Bucinsky et al. [26]. The accuracy of the ML predicted docking scores of **W** set compounds is presented including the time scales (docking vs. ML).

2. Methods & computational details

The 3D structure of SARS-CoV-2 $3CL^{pro}$ determined at room temperature (PDB ID: 6WQF) [32] was downloaded from the RCSB protein data bank [33]. The protease was stripped of water molecules, retaining only a single water molecule near His41 and Asp187 residues facilitating charge stabilization interactions on nearby residues [32]. The pdbqt file format of the 6WQF protein structure for the **W** set docking study has been prepared with AutoDockTools-1.5.7 as given by Bucinsky et al. [26] (keeping only polar hydrogens and using Gasteiger charges). Semi-flexible molecular docking calculations were performed using Autodock4.2.6 [34,35] with compounds having assigned Gasteiger charges. Potential maps were calculated in a $90 \times 90 \times 90$ grid box, with a resolution of 0.275 Å, centered at x, y, z = (−20, −5, 15) Å. Fifty runs of the Lamarckian genetic algorithm have been performed with the total number of individuals in generation, maximum populations, and energy evaluations set to 300, 27,000, and 30,000,000, respectively. The resulting poses were clustered with a 2.0 Å tolerance and the hydrogen bond pattern was analyzed with the AutodockTools scripts [34,35]. Schematic 2D diagrams of the predicted binding mode were prepared in LigPlot+ software [36].

To evaluate the docking scores reliability further, five compounds with the lowest 6WQF docking scores were selected for molecular dynamics (MD) simulations in GROMACS2018.7 [37–40] according to the original **S** set study of Steklac et al. [31]. In addition, MD simulations accounted also for Hentriacontane ($C_{31}H_{64}$), which achieved the 11th best docking score (for reasons elucidated in further texts). MD simulations of each compound accounted for five distinguished (randomly initialized) trajectories, see Supplementary Materials for further details.

Absorption, distribution, metabolism, excretion (ADME) parameters as well as other physicochemical descriptors, lipophilicity, solubility, pharmacokinetics, and druglikeness. of the studied **W** set compounds were computed from a list of SMILES codes using the SwissADME website [41], see the Supplementary Materials for the full SwissADME csv file output.

Machine learning predictions of the docking scores were carried out using TensorFlow [42], XGBoost [43], and SchNetPack [44] utilizing the

S training set for the ML train process itself according to Bucinsky et al. [26]. All **W** set docking scores, and their ML predictions are accounted for in the Supplementary Materials.

3. Results

3.1. Docking scores

Molecular docking approaches can be used to obtain structural information about the ligand-protein complexes and the binding affinity of the particular ligand-protein pair [45]. Although the predicted binding affinities vary greatly depending on the various docking protocols, docking scores calculated with the same docking protocol allow for a certain degree of comparison between the studied compound sets. The docking results for the **W** set of Jablonsky et al. [29] (red crosses) are compared with the results of the **S** set presented by Steklac et al. [31] (blue solid circles), see Fig. 1a and S1a. The docking scores correlation with ESOL log S solubility prediction is shown in Fig. 1b. The complete results of the **W** set are given in the Supplementary Materials. Compounds with docking scores below −13 kcal/mol are on par with antiviral drug candidates specifically designed to target SARS-CoV-2 $3CL^{pro}$, such as peptidomimetic aldehydes 11a/11b [16] (−13.48/−12.89 kcal/mol [31]), and have been considered suitable candidates for further derivatization and possible drug repurposing. There are four compounds in the **W** set (lariciresinol-9-p-coumarate, β-sitosterol acetate, sesquipinsapol B, and Campesterol) that have achieved this score, see Table 1, while 11 compounds have achieved a docking score below −11 kcal/mol, see Table 1 and Supplementary Materials. In addition, ca. half of the studied compounds have achieved a docking score below −8 kcal/mol and a quarter below −10 kcal/mol, see Supplementary Materials. It is worthwhile to highlight that the best compound of the **W** set, (+)-lariciresinol 9′-p-coumarate (CID 11497085), has achieved a better docking score than the best compounds compiled by Steklac et al. [31]. The docking pose of the best scoring compound from the **W** data set ((+)-lariciresinol 9′-p-coumarate; CID 11497085) is presented in Fig. 2.

Interestingly, the docking scores of the **W** set have a vertical structure which suggests that these compounds are metabolites of a similar size (molecular weight, MW), see Fig. 1a and S1a. Nevertheless, the docking scores are seen to differ, thus allowing one to study the structure – functionality relation in these sets. For instance, 18 compounds are identified with MW of 136.23 Da (1,5-cyclodecadiene, 3-vinylcycloocten, tricyclene, α-thujene, α-pinene, α-fenchene, camphene, sabinene, β-pinene, myrcene, α-phellandrene, 3-carene, terpinolene, α-terpinene, (+)-β-phellandrene, limonene, *Z*-β-ocimine, γ-terpinene), 7 compounds have MW 154.25 Da, 38 compounds have MW 204.35 Da, 10 compounds have MW 222.37 Da, 6 compounds have MW 290.5 Da, and 6 compounds have MW 316.5 Da, see Supplementary Materials. The compounds studied in the **W** set form a well-defined set with respect to their MW, ranging from 100 to 550 Da, with only one exception, the tannic acid (CID 16129778) with MW of 1701.20 Da (see Fig. S1b). The

Table 1
Top 10 scoring compounds from the **W** data set identified by their CID in PubChem database and trivial name, together with achieved docking score and list of predicted interacting amino acids.

CID	Compound name	Score [kcal/mol]	Predicted interacting amino acids
11497085	(+)-Lariciresinol 9′-p-coumarate	−15.12	Thr25, Ser144, His163, Glu166, Thr190
5354503	β-sitosterol acetate	−14.14	Thr26
101767126	Sesquipinsapol B	−13.39	Thr24, Asn142, Gly143, Glu166, Thr190
173183	Campesterol	−13.25	Thr26
101928787	Ehletianol C	−12.93	Ser144, His163, Glu166, Gln189
13783149	Stigmastan-3,5-diene	−12.38	–
5281712	Astringin	−12.01	Phe140, Asn142, Ser144, His163, Thr190, Gln192
70698172	Vladinol D	−11.77	Ser144, His163, Glu166, Gln189, Thr190
38347252	Junicedric acid	−11.47	Asn142, Gly143, Thr190, Gln192
5281716	Isorhapontin	−11.39	Gly143, Ser144, His163, Glu166, Thr190, Gln189

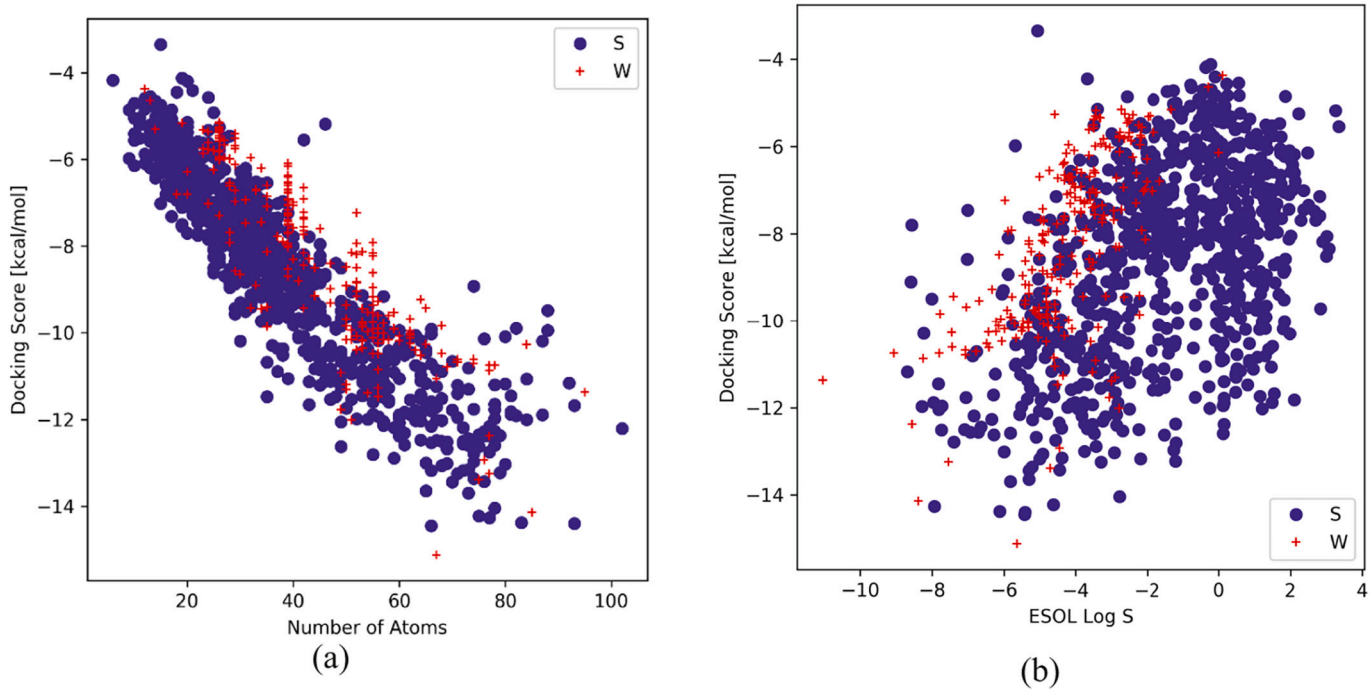

Fig. 1. Docking scores of the **W** (red crosses) and **S** (blue dots) sets with respect, to the number of atoms (a), and ESOL log S solubility (b). Tannic acid is not shown in these figures, as it is outside of the displayed range. (For interpretation of the references to colour in this figure legend, the reader is referred to the web version of this article.)

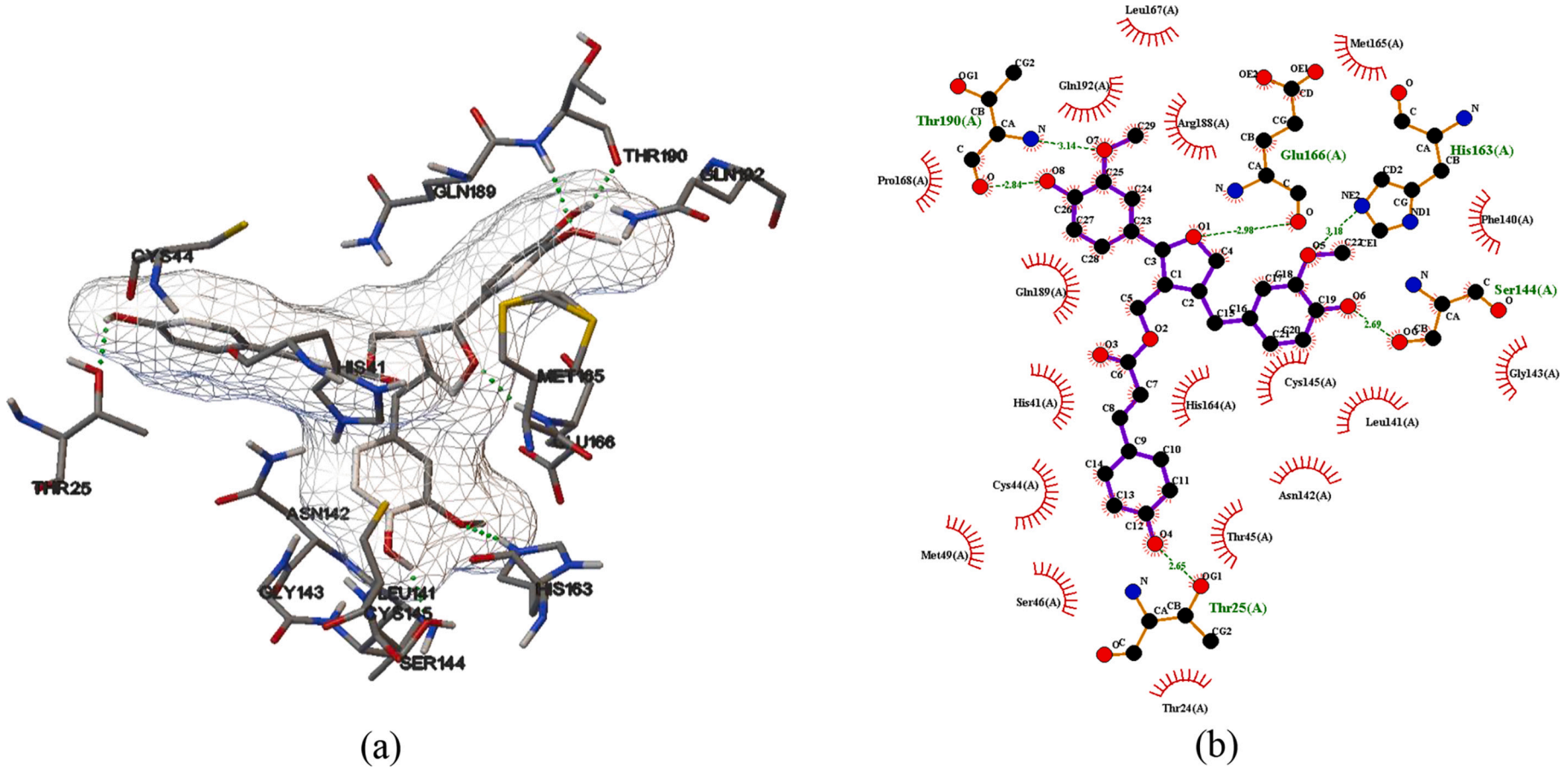

Fig. 2. The putative docking poses of the best scoring compound of the **W** data set (CID 11497085) in (a) 3D and (b) 2D representation. The amino acids participating in the formation of hydrogen bonds are fully drawn and the predicted hydrogen bonds are represented by dashed green lines (a). Amino acids that lie in proximity of the docked compound, thus participating in non-covalent pair-wise interactions, are depicted by red arches (b). (For interpretation of the references to colour in this figure legend, the reader is referred to the web version of this article.)

docking score (−6.15 kcal/mol) of this compound was calculated with a restricted number of torsional degrees of freedom, as its maximum number exceeded the limits of the docking software. Therefore, the rotation around the bonds to alcohol moieties on terminal benzenes, as well as around the bonds to terminal carbonyl groups, had been restricted, thus fixing the geometry of 3,4,5-trihydroxybenzoates.

The number of predicted hydrogen bonds between the docked compound and $3CL^{pro}$ ranges from 0 to 8, with as much as 95 compounds not having any predicted bonding pattern, while 48 compounds have only one predicted hydrogen bond predicted. It should be noted that up to 164 **W** compounds do not have polar hydrogens, suggesting a strong aliphatic character within this set. The ability of such compounds to form hydrogen bonds is thus severely limited, i.e., such compounds can act only as a hydrogen bond acceptor if, e.g., a keto moiety is present. In this case, the hydrogen bonding pattern is linked to predicted inhibitory activity, as there is a visible decrease in the docking score with respect to the number of predicted hydrogen bonds, see Fig. 3a. The commonly predicted hydrogen bonds are formed with the amino acids from S3-S5 subsides (Glu166, Gln189, Thr190) that can tolerate various functionalities. Direct interactions with the amino acids that form the catalytic dyad (His41, Cys145) have been predicted in two cases (CID 445154 and CID 638034). Hence, the **W** set compounds would in the vast majority act as steric inhibitors, rather than direct inhibitors of the catalytic center of $3CL^{pro}$.

Furthermore, it should be noted that compounds from this data set have achieved excellent values of ligand efficacy (the docking score divided by the number of non-hydrogen atoms in the compound) compared to compounds from the **S** set with corresponding molecular weights (number of atoms), see Fig. 3b. This suggests that their interactions with cavity atoms are rather strong, and the docking score is not driven by the number of the hydrogen interactions themselves. Such compounds offer a potential target for further structure derivatization to increase the inhibitory activity and/or improve other physicochemical properties.

3.2. Solubility and druglikeness

Although the **S** set compounds show better solubility predictions compared to **W**, the best docking compound ranks at the solubility limit of −6, see Fig. 1b. In addition, several **W** set compounds have the ESOL log S value better (larger) than −4 and docking scores below −10 kcal/mol (astringin, vladinol D, isorhapontin, piceid, lariciresinol, hydroxymatairesinol, retinol acetate, isolariciresonol), see Fig. 1b. It should be noted that even compounds from the **S** set that are considered suitable therapeutics show solubility predictions with pure ESOL log S rankings of −8. The druglikeness (SwissADME radar plots) potential of the best compounds from the **S** and **W** set is shown in Figs. S2 and S3 for brevity. The **W** set compounds β-sitosterol acetate, Campesterol, and Stigmastan-3,5-diene, show a considerably different pattern with respect to INSATU, POLAR criteria, and solubility criteria. The radar plots of the remaining **W** set compounds in Fig. S3 show a behavior similar to the best docking compound radar plots of the **S** set in Fig. S2. Interestingly, the 11th best docking score in the **W** set achieved the aliphatic hydrocarbon compound, Hentriacontane ($C_{31}H_{64}$) which has the most negative (−11.0) ESOL log S value.

Although several compounds contained in the **W** set did not reach the top docking scores, their antiviral effects and inhibitory potential against the main protease of the SARS-CoV-2 virus, $3CL^{pro}$, have been demonstrated in several studies. Bahun et al. [46] dealt with an application of molecular docking as well as molecular dynamics supported by in vitro assays to determine the inhibitory potential of various plant polyphenols against the $3CL^{pro}$ protease. Resveratrol (CID 445154) and quercetin (CID 5280343) were among the five compounds that showed >50% $3CL^{pro}$ inhibition. These substances have obtained docking scores below −8 kcal/mol in our study, namely resveratrol −8.58 kcal/mol and quercetin −9.43 kcal/mol, see Supplementary Materials. There is a growing number of publications that have reported that resveratrol has promising therapeutic effects against lung diseases by inhibiting oxidative stress, inflammation, aging, fibrosis, and cancer [47]. It was suggested that it can act as an inhibitor of the ACE2 receptor and prevent the spike glycoprotein:ACE2 complex formation and hence the entry of

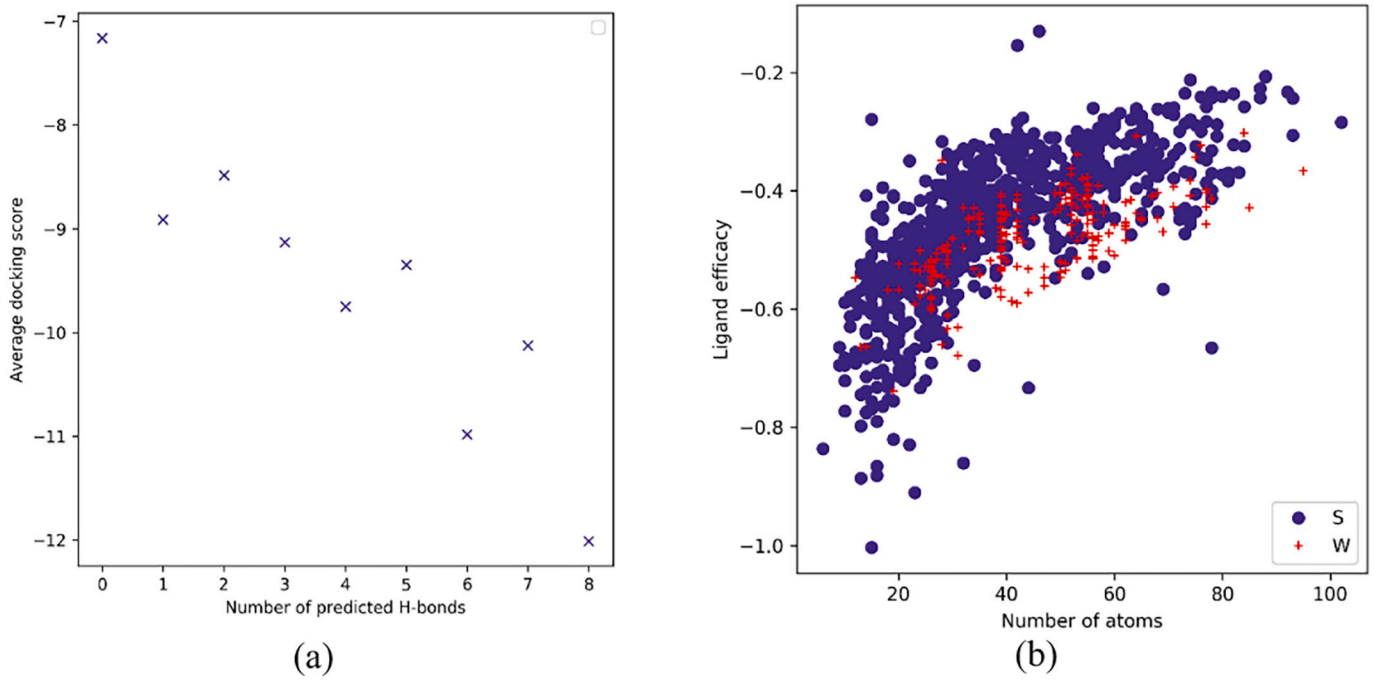

Fig. 3. (a) Average docking score according to the number of predicted hydrogen bonds between the protein target and the docked compound; (b) ligand efficacy of the **W** (red dots) and **S** (blue dots) sets. Tannic acid is not shown in this figure as it is outside of the displayed range. (For interpretation of the references to colour in this figure legend, the reader is referred to the web version of this article.)

the virion into host cells [48]. Quercetin can protect against SARS-CoV-2 infection by impeding virion entry into host cells by modifying spike glycoprotein and/or ACE2, or repressing replication inside the cells by inhibiting $3CL^{pro}$ [49–51]. Based on the results of a randomized controlled study presented by Shohan et al. [52], it can be stated that quercetin may be therapeutically effective in reducing the time to clinical improvement in combination with antiviral drugs. Among all compounds, epicatechin (CID 72276) and kempferol (CID 5280863) were predicted to exert the highest druglikeness and lowest toxicity potentials in the work of Al-Shuhaib et al. [20]. Epicatechin and catechin (with a docking score against $3CL^{pro}$ of −9.85 and −9.42 kcal/mol, respectively) could also act as potential inhibitory agents to prevent binding of ACE2 with the SARS-CoV-2 spike glycoprotein [20,53].

3.3. Molecular dynamics

Molecular dynamics simulations have been employed to overcome the rigid protein picture and to verify the conformational stability of a compound-protein complex in water solvent. Five MD runs of the top scoring compound, (+)-Lariciresinol 9′-p-coumarate (CID: 11497085), have been carried out and validated by RMSD of compounds' heavy atoms with respect to the protein backbone and the number of hydrogen bonds; see Fig. 4.

Two runs achieve equilibrium at the start of the MD simulation with averaged RMSD value ca. 0.3 nm, indicating only minor conformational changes that can be attributed to small drifts in the trajectory, see Fig. 2a. Three additional MD runs manifest non-negligible motion of the compound in the protein cavity. Two runs exhibit RMSD values oscillating around 0.6 nm, whereas the highest observed RMSD of the final simulation is ca. 1.0 nm. Upon visualization of MD trajectories, it is revealed that an increase in RMSD values up to 0.6 nm is associated with an elevation of the methyl (E)-3-(4-hydroxyphenyl)prop-2-enoate moiety from the protein surface. A further increase to 1.0 nm originates from its rotation around the bond with the central furan group. However, both 4-hydroxy-3-methoxyphenyl moieties remain firmly attached to the amino acid residues in the protein cavity, as illustrated by the time evolution of the number of hydrogen bonds; see Fig. 4b. The number of hydrogen bonds/interactions within the MD simulation is ranging from 2 (for runs exhibiting higher RMSD) to 8 (for runs with a higher conformational stability). One hydrogen bond, between hydroxyl hydrogen on methyl (E)-3-(4-hydroxyphenyl)prop-2-enoate moiety and Thr25, is consistently broken during all MD simulations. This indicates a favoring conformational stability of the compound in the protein cavity and proves its potential to inhibit the active site of the SARS-CoV-2 $3CL^{pro}$ unit.

A similar approach has been applied to the remaining four best scoring compounds (CIDs: 5354503, 101767126, 173183, 10192877), as well as to Hentriacontane (CID: 12410), with the graphical representations found in the Supplementary Materials; see Fig. S4. Inclusion of Hentriacontane (11th best docking score) serves as an illustration of the time evolution of the monitored parameters for a compound with no conformational stability in the cavity pocket. The absence of potential hydrogen bond donor/acceptor groups does not allow the formation of hydrogen bonds, and its high rotational flexibility leads to a gradual increase in RMSD value that does not reach equilibrium during the MD simulations, see Fig. S4.

3.4. Machine learning

ML prediction of docking scores is presented in Fig. 5 and Table 2. It was found that the **S** set trained ML approaches can predict the **W** set docking scores with a reasonable accuracy. SchNetPack yields the best slope (k) value and the worst mean square error (MSE), and R^2. The standard error of the docking calculations is assumed to be between 2 and 3 kcal/mol [34]. Five, five, and nine compounds have the docking score deviation, expected vs. predicted, larger than 2 kcal/mol for TensorFlow, XGBoost and SchNetPack (one, two, and one compound larger than 3 kcal/mol), respectively. Predictions of the docking score of tannic acid are the most deviated. The absolute error for this compound is 8.683, 5.084 and 14.397 kcal/mol for TensorFlow, XGBoost and SchNetPack, respectively. The prediction of docking scores of compounds with more than 120 atoms was found problematic in the original work of Bucinsky et al. [26], which is confirmed herein for the case of the tannic acid. The agreement between the AutoDock calculated (expected) and ML predicted docking scores improves after leaving this compound out of the linear correlation, see Table 2.

Aside from the achieved accuracy of the docking scores prediction, main ML advantage is the timing. The AutoDock calculation of **W** set docking scores took 28 days and 4 h of CPU time (average CPU time per compound was ca. 3 h). On the contrary, the ML prediction of the **W** set docking scores is at least five orders of magnitude faster than the molecular docking. The process of submitting the **W** set .xyz file into the descriptor and prediction protocol of TensorFlow took 14.6 s, i.e., 14.3 s for descriptor generation and 0.3 s for the actual prediction of docking

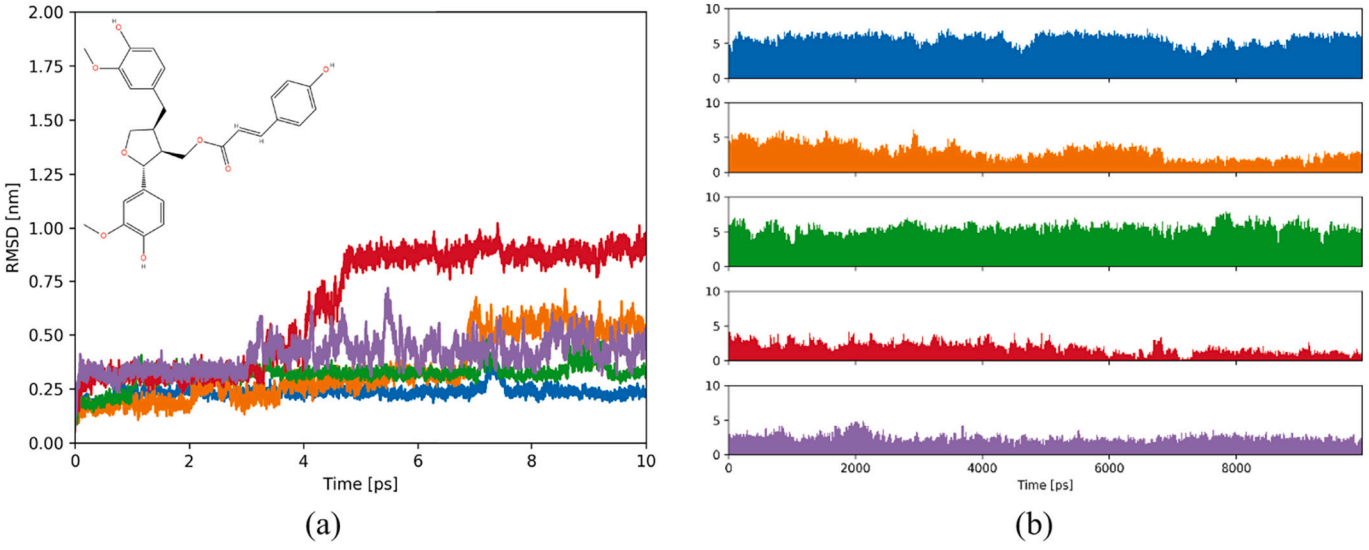

Fig. 4. MD time plot evolution of: RMSD values of compounds' heavy atoms with respect to the protein backbone (a); the number of hydrogen bonds to SARS-CoV-2 $3CL^{pro}$ (b); of (+)-Lariciresinol 9′-p-coumarate (CID: 11497085).

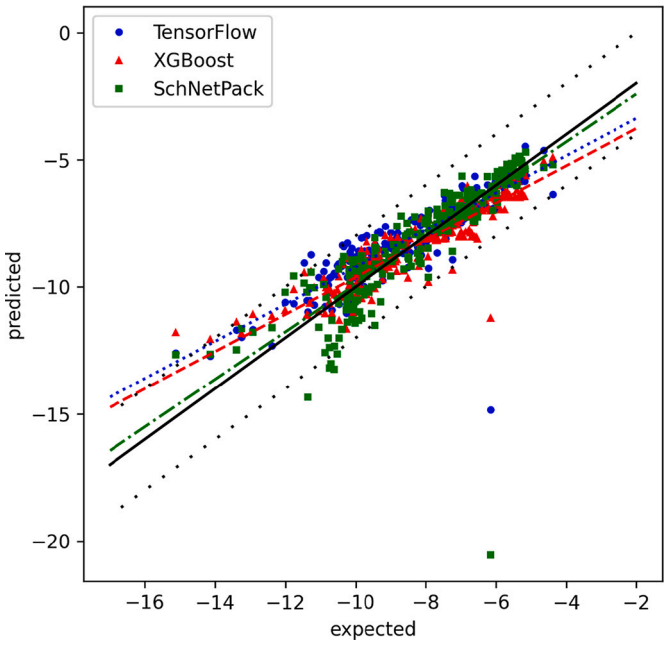

Fig. 5. ML docking score prediction comparing to the expected AutoDock reference: blue circles TensorFlow (blue dotted line), red triangles XGBoost (red dashed line), and green squares SchNetPack (green dash-dotted line). Ideal y = x line is black solid and black 'loosely dotted' lines define the y = x ± 2 kcal/mol interval range. (For interpretation of the references to colour in this figure legend, the reader is referred to the web version of this article.)

Table 2
Correlation between ML docking score prediction and the expected AutoDock reference: linear fit (y = k.x + q), including standard deviations and R^2, and MSE. Timings (in CPU seconds) for the **W** set prediction are amended and split into descriptor generation and score prediction, where appropriate.

W set						
Approach	k	q	σ_k	σ_q	R^2	MSE
TensorFlow	0.731	−1.917	0.026	0.221	0.772	1.002
XGBoost	0.731	−2.314	0.021	0.182	0.833	0.715
SchNetPack	0.935	−0.555	0.041	0.350	0.689	1.570

W set without the Tannic acid (CID 16129778)						
Approach	k	q	se	ie	R2	MSE
TensorFlow	0.750	−1.721	0.019	0.159	0.875	0.683
XGBoost	0.741	−2.211	0.019	0.164	0.865	0.607
SchNetPack	0.967	−0.222	0.027	0.232	0.844	0.687

Timings		
Approach	Descriptor generation	Score prediction
TensorFlow	14.3	0.322
XGBoost	11.1	0.085
SchNetPack	–	10.5[a]

[a] This is the total prediction time, as SchNetPack does not separate descriptor generation and score prediction times.

scores, see Table 2. In the case of XGBoost, the prediction took 11.2 s, i.e. 11.1 s for descriptor generation and 0.1 s for the actual prediction of docking scores, see Table 2. Finally, the total prediction time for SchNetPack docking scores was 10.5 s, see Table 2.

4. Conclusions

The SARS-CoV-2 pandemic shows the danger of zoonotic viruses for humankind and illustrates the need for the treatment of such diseases. Moreover, the rate of virus mutation indicates the necessity for quick drug search and discovery, which can be facilitated by fast and cost-efficient computational methods. Virtual screening can lead to discovery of potential virus inhibitors or their precursors, either from sets of commonly used therapeutic agents or from naturally occurring compounds.

Herein, we have employed *in silico* molecular docking methods and machine learning prediction protocols to determine the binding affinity pattern to SARS-CoV-2 main protease $3CL^{pro}$ of 234 naturally occurring compounds from softwood bark and to identify their potential inhibition activity. Compounds such as (+)-lariciresinol 9′-p-coumarate, β-sitosterol acetate, sesquipinsapol B and campesterol all exhibit an excellent docking score and their predicted free energies of binding (docking scores) are comparable with those of the known $3CL^{pro}$ inhibitors, indicating their promise as potential drug candidates against COVID-19. In addition, 50% of the compounds can be identified as suitable for a further derivatization. However, it is important to consider the limitations of the molecular docking approach, and thus further validation of the predicted affinity by experimental means is highly warranted for the best scoring compounds. The semi-flexible molecular docking results have been verified for the five best scoring compounds using MD simulations. The MD results show a favoring conformational stability of these compounds in the SARS-CoV-2 $3CL^{pro}$ protein cavity.

Machine learning prediction of the docking score is found to be fast and reliable for a quick pick-up of suitable compounds which number can be further reduced by means of more accurate, but time-consuming methods (such as molecular docking or molecular dynamics), prior to the in vitro trials.

CRediT authorship contribution statement

Michal Jablonský: Data curation, Writing – original draft. **Marek Štekláč:** Data curation, Writing – original draft. **Veronika Majová:** Writing – review & editing. **Marián Gall:** Data curation, Writing – review & editing. **Ján Matúška:** Data curation, Writing – review & editing. **Michal Pitoňák:** Data curation, Writing – review & editing. **Lukáš Bučinský:** Writing – original draft.

Declaration of Competing Interest

The authors declare that they have no known competing financial interests or personal relationships that could have appeared to influence the work reported in this paper.

Acknowledgements

This publication was supported by the Slovak Research and Development Agency under the contract APVV-20-0213 and APVV-20-0127, and by the generous support under the Operational Program Integrated Infrastructure for the project: "Strategic research in the field of SMART monitoring, treatment, and preventive protection against coronavirus (SARS-CoV-2)," Project no. 313011ASS8, co-financed by the European Regional Development Fund (ERDF). Further financial support was obtained from the Slovak Grant Agency VEGA under contract nos. 1/0718/19, 1/0777/19, and 1/0139/20. We thank the Computing Centre of the Slovak Academy of Sciences and the HPC centre at the Slovak University of Technology in Bratislava, which are associated in the Slovak Infrastructure of High-Performance Computing (SIVVP Project, ITMS codes 26210120002 and 26230120002, funded by ERDF), for computing facilities. LB is grateful to Ministry of Education, Science, Research and Sport of the Slovak Republic for funding within the scheme "Excellent research teams".

Appendix A. Supplementary data

Supplementary data to this article can be found online at https://doi.org/10.1016/j.bpc.2022.106854.

References

[1] M. Rastogi, N. Pandey, A. Shukla, S.K. Singh, SARS coronavirus 2: from genome to infectome, Respir. Res. 21 (2020) 318, https://doi.org/10.1186/s12931-020-01581-z.

[2] T.P. Velavan, C.G. Meyer, The COVID-19 epidemic, Tropical Med. Int. Health 25 (2020) 278–280, https://doi.org/10.1111/tmi.13383.

[3] K.F. Azim, S.R. Ahmed, A. Banik, M.M.R. Khan, A. Deb, S.R. Somana, Screening and druggability analysis of some plant metabolites against SARS-CoV-2: an integrative computational approach, Informatics Med. Unlocked. 20 (2020), 100367, https://doi.org/10.1016/j.imu.2020.100367.

[4] H. González-Pacheco, R. Gopar-Nieto, G.-M. Jiménez-Rodríguez, D. Manzur-Sandoval, J. Sandoval, A. Arias-Mendoza, Bilateral spontaneous pneumothorax in SARS-CoV-2 infection: A very rare, life-threatening complication, Am. J. Emerg. Med. 39 (2021), https://doi.org/10.1016/j.ajem.2020.07.018, 258.e1–258.e3.

[5] Y.-M. Kim, E.-C. Shin, Type I and III interferon responses in SARS-CoV-2 infection, Exp. Mol. Med. 53 (2021) 750–760, https://doi.org/10.1038/s12276-021-00592-0.

[6] T. Singhal, A Review of Coronavirus Disease-2019 (COVID-19), Indian J. Pediatr. 87 (2020) 281–286, https://doi.org/10.1007/s12098-020-03263-6.

[7] L. Zou, F. Ruan, M. Huang, L. Liang, H. Huang, Z. Hong, J. Yu, M. Kang, Y. Song, J. Xia, Q. Guo, T. Song, J. He, H.-L. Yen, M. Peiris, J. Wu, SARS-CoV-2 viral load in upper respiratory specimens of infected patients, N. Engl. J. Med. 382 (2020) 1177–1179, https://doi.org/10.1056/NEJMc2001737.

[8] C. Wu, Y. Liu, Y. Yang, P. Zhang, W. Zhong, Y. Wang, Q. Wang, Y. Xu, M. Li, X. Li, M. Zheng, L. Chen, H. Li, Analysis of therapeutic targets for SARS-CoV-2 and discovery of potential drugs by computational methods, Acta Pharm. Sin. B 10 (2020) 766–788, https://doi.org/10.1016/j.apsb.2020.02.008.

[9] H. Islam, A. Rahman, J. Masud, D.S. Shweta, Y. Araf, M.A. Ullah, S.M. Al Sium, B. Sarkar, A Generalized Overview of SARS-COV-2: Where Does the Current Knowledge Stand? vol. 17, 2020, https://doi.org/10.29333/ejgm/8258.

[10] Q. Li, C. Kang, Progress in developing inhibitors of SARS-CoV-2 3C-like protease, Microorganisms. 8 (2020), https://doi.org/10.3390/microorganisms8081250.

[11] A.I. Petushkova, A.A.J. Zamyatnin, Papain-like proteases as Coronaviral drug targets: current inhibitors, opportunities, and limitations, Pharmaceuticals (Basel). 13 (2020), https://doi.org/10.3390/ph13100277.

[12] A. Zumla, J.F.W. Chan, E.I. Azhar, D.S.C. Hui, K.-Y. Yuen, Coronaviruses — drug discovery and therapeutic options, Nat. Rev. Drug Discov. 15 (2016) 327–347, https://doi.org/10.1038/nrd.2015.37.

[13] E. Tejera, C.R. Munteanu, A. López-Cortés, A. Cabrera-Andrade, Y. Pérez-Castillo, Drugs repurposing using QSAR, docking and molecular dynamics for possible inhibitors of the SARS-CoV-2 Mpro protease, Molecules. 25 (2020), https://doi.org/10.3390/molecules25215172.

[14] Z. Jin, X. Du, Y. Xu, Y. Deng, M. Liu, Y. Zhao, B. Zhang, X. Li, L. Zhang, C. Peng, Y. Duan, J. Yu, L. Wang, K. Yang, F. Liu, R. Jiang, X. Yang, T. You, X. Liu, X. Yang, F. Bai, H. Liu, X. Liu, L.W. Guddat, W. Xu, G. Xiao, C. Qin, Z. Shi, H. Jiang, Z. Rao, H. Yang, Structure of Mpro from SARS-CoV-2 and discovery of its inhibitors, Nature. 582 (2020) 289–293, https://doi.org/10.1038/s41586-020-2223-y.

[15] S.A. Khan, K. Zia, S. Ashraf, R. Uddin, Z. Ul-Haq, Identification of chymotrypsin-like protease inhibitors of SARS-CoV-2 via integrated computational approach, J. Biomol. Struct. Dyn. (2020) 1–10, https://doi.org/10.1080/07391102.2020.1751298.

[16] W. Dai, B. Zhang, X.-M. Jiang, H. Su, J. Li, Y. Zhao, X. Xie, Z. Jin, J. Peng, F. Liu, C. Li, Y. Li, F. Bai, H. Wang, X. Cheng, X. Cen, S. Hu, X. Yang, J. Wang, X. Liu, G. Xiao, H. Jiang, Z. Rao, L.-K. Zhang, Y. Xu, H. Yang, H. Liu, Structure-based design of antiviral drug candidates targeting the SARS-CoV-2 main protease, Science (80-.) 368 (2020), https://doi.org/10.1126/science.abb4489, 1331 LP – 1335.

[17] M. Jablonský, F. Kreps, A. Ház, J. Šima, J. Jablonský, Green solvents, plant metabolites, and COVID-19: challenges and perspectives, BioResources. 16 (2021) 4667–4670, https://doi.org/10.15376/biores.16.3.4667-4670.

[18] A.D. Fuzimoto, C. Isidoro, The antiviral and coronavirus-host protein pathways inhibiting properties of herbs and natural compounds - additional weapons in the fight against the COVID-19 pandemic? J. Tradit. Complement. Med. 10 (2020) 405–419, https://doi.org/10.1016/j.jtcme.2020.05.003.

[19] M.S.A. Parvez, K.F. Azim, A.S. Imran, T. Raihan, A. Begum, T.S. Shammi, S. Howlader, F.R. Bhuiyan, M. Hasan, Virtual Screening of Plant Metabolites against Main Protease, RNA-Dependent RNA Polymerase and Spike Protein of SARS-CoV-2: Therapeutics Option of COVID-19. http://arxiv.org/abs/2005.11254, 2020.

[20] M.B.S. Al-Shuhaib, H.O. Hashim, J.M.B. Al-Shuhaib, Epicatechin is a promising novel inhibitor of SARS-CoV-2 entry by disrupting interactions between angiotensin-converting enzyme type 2 and the viral receptor binding domain: a computational/simulation study, Comput. Biol. Med. 141 (2021), 105155, https://doi.org/10.1016/j.compbiomed.2021.105155.

[21] M. Tahir Ul Qamar, S.M. Alqahtani, M.A. Alamri, L.-L. Chen, Structural basis of SARS-CoV-2 3CL(pro) and anti-COVID-19 drug discovery from medicinal plants, J. Pharm. Anal. 10 (2020) 313–319, https://doi.org/10.1016/j.jpha.2020.03.009.

[22] M. Yonesi, A. Rezazadeh, Plants as a Prospective Source of Natural Anti-viral Compounds and Oral Vaccines Against COVID-19 Coronavirus, 2020, https://doi.org/10.20944/PREPRINTS202004.0321.V1.

[23] L.I. da Silva Hage-Melim, L.B. Federico, N.K.S. de Oliveira, V.C.C. Francisco, L. C. Correia, H.B. de Lima, S.Q. Gomes, M.P. Barcelos, I.A.G. Francischini, C.H.T. de Paula da Silva, Virtual screening, ADME/Tox predictions and the drug repurposing concept for future use of old drugs against the COVID-19, Life Sci. 256 (2020), 117963, https://doi.org/10.1016/j.lfs.2020.117963.

[24] A. Acharya, R. Agarwal, M.B. Baker, J. Baudry, D. Bhowmik, S. Boehm, K.G. Byler, S.Y. Chen, L. Coates, C.J. Cooper, O. Demerdash, I. Daidone, J.D. Eblen, S. Ellingson, S. Forli, J. Glaser, J.C. Gumbart, J. Gunnels, O. Hernandez, S. Irle, D. W. Kneller, A. Kovalevsky, J. Larkin, T.J. Lawrence, S. LeGrand, S.-H. Liu, J. C. Mitchell, G. Park, J.M. Parks, A. Pavlova, L. Petridis, D. Poole, L. Pouchard, A. Ramanathan, D.M. Rogers, D. Santos-Martins, A. Scheinberg, A. Sedova, Y. Shen, J.C. Smith, M.D. Smith, C. Soto, A. Tsaris, M. Thavappiragasam, A. F. Tillack, J.V. Vermaas, V.Q. Vuong, J. Yin, S. Yoo, M. Zahran, L. Zanetti-Polzi, Supercomputer-Based Ensemble Docking Drug Discovery Pipeline with Application to Covid-19 60, 2020, pp. 5832–5852, https://doi.org/10.1021/acs.jcim.0c01010.

[25] R. Batra, H. Chan, G. Kamath, R. Ramprasad, M.J. Cherukara, S.K.R. S. Sankaranarayanan, Screening of Therapeutic Agents for COVID-19 Using Machine Learning and Ensemble Docking Studies 11, 2020, pp. 7058–7065, https://doi.org/10.1021/acs.jpclett.0c02278.

[26] L. Bucinsky, D. Bortňák, M. Gall, J. Matúška, V. Milata, M. Pitoňák, M. Štekláč, D. Végh, D. Zajaček, Machine learning prediction of 3CLpro SARS-CoV-2 docking scores, Comput. Biol. Chem. 98 (2022), 107656, https://doi.org/10.1016/j.compbiolchem.2022.107656.

[27] M. Smith, J. Smith, Repurposing Therapeutics for COVID-19: Supercomputer-Based Docking to the SARS-CoV-2 Viral Spike Protein and Viral Spike Protein-Human ACE2 Interface, 2020, https://doi.org/10.26434/chemrxiv.11871402.v4.

[28] F. Gentile, V. Agrawal, M. Hsing, A.-T. Ton, F. Ban, U. Norinder, M.E. Gleave, A. Cherkasov, Deep docking: a deep learning platform for augmentation of structure based, Drug Discovery 6 (2020) 939–949, https://doi.org/10.1021/acscentsci.0c00229.

[29] M. Jablonsky, J. Nosalova, A. Sladkova, A. Haz, F. Kreps, J. Valka, S. Miertus, V. Frecer, M. Ondrejovic, J. Sima, I. Surina, Valorisation of softwood bark through extraction of utilizable chemicals. A review, Biotechnol. Adv. 35 (2017) 726–750, https://doi.org/10.1016/j.biotechadv.2017.07.007.

[30] P. Strižincová, M. Jablonsky, M. Lelovský, Bioactive compounds of softwood bark as potential agents against human diseases include the SARS-CoV-2 virus, Biointerface Res. Appl. Chem. 12 (2021) 5860–5869, https://doi.org/10.33263/BRIAC125.58605869.

[31] M. Štekláč, D. Zajaček, L. Bučinský, 3CLpro and PLpro affinity, a docking study to fight COVID19 based on 900 compounds from PubChem and literature. Are there new drugs to be found? J. Mol. Struct. 1245 (2021), 130968 https://doi.org/10.1016/j.molstruc.2021.130968.

[32] D.W. Kneller, G. Phillips, H.M. O'Neill, R. Jedrzejczak, L. Stols, P. Langan, A. Joachimiak, L. Coates, A. Kovalevsky, Structural plasticity of SARS-CoV-2 3CL Mpro active site cavity revealed by room temperature X-ray crystallography, Nat. Commun. 11 (2020) 3202, https://doi.org/10.1038/s41467-020-16954-7.

[33] H.M. Berman, J. Westbrook, Z. Feng, G. Gilliland, T.N. Bhat, H. Weissig, I. N. Shindyalov, P.E. Bourne, The Protein Data Bank, Nucleic Acids Res. 28 (2000) 235–242, https://doi.org/10.1093/nar/28.1.235.

[34] G.M. Morris, R. Huey, W. Lindstrom, M.F. Sanner, R.K. Belew, D.S. Goodsell, A. J. Olson, AutoDock4 and AutoDockTools4: automated docking with selective receptor flexibility, J. Comput. Chem. 30 (2009) 2785–2791, https://doi.org/10.1002/jcc.21256.

[35] M.F. Sanner, Python: a programming language for software integration and development, J. Mol. Graph. Model. 17 (1999) 57–61.

[36] A.C. Wallace, R.A. Laskowski, J.M. Thornton, LIGPLOT: a program to generate schematic diagrams of protein-ligand interactions, Protein Eng. 8 (1995) 127–134, https://doi.org/10.1093/protein/8.2.127.

[37] E. Lindahl, B. Hess, D. van der Spoel, GROMACS 3.0: a package for molecular simulation and trajectory analysis, Mol. Model. Annu. 7 (8) (2001) 306–317, https://doi.org/10.1007/s008940100045.

[38] H. Bekker, et al., Gromacs - a parallel computer for molecular-dynamics simulations, in: 4th International Conference on Computational Physics (PC 92), World Scientific Publishing, SINGAPORE, 1993, pp. 22–256. BT-PHYSICS COMPUTING '92.

[39] H.J.C. Berendsen, D. van der Spoel, R. van Drunen, GROMACS: a message-passing parallel molecular dynamics implementation, Comput. Phys. Commun. 91 (1) (1995) 43–56, https://doi.org/10.1016/0010-4655(95)00042-E.

[40] D. Van Der Spoel, E. Lindahl, B. Hess, G. Groenhof, A.E. Mark, H.J.C. Berendsen, GROMACS: fast, flexible, and free, J. Comput. Chem. 26 (16) (2005) 1701–1718, https://doi.org/10.1002/jcc.20291.

[41] A. Daina, O. Michielin, V. Zoete, SwissADME: a free web tool to evaluate pharmacokinetics, drug-likeness and medicinal chemistry friendliness of small molecules, Sci. Rep. 7 (1) (2017) 42717, https://doi.org/10.1038/srep42717.

[42] M. Abadi, A. Agarwal, P. Barham, E. Brevdo, Z. Chen, C. Citro, G.S. Corrado, A. Davis, J. Dean, M. Devin, S. Ghemawat, I. Goodfellow, A. Harp, G. Irving, M. Isard, Y. Jia, R. Jozefowicz, L. Kaiser, M. Kudlur, J. Levenberg, D. Mane, R. Monga, S. Moore, D. Murray, C. Olah, M. Schuster, J. Shlens, B. Steiner, I. Sutskever, K. Talwar, P. Tucker, V. Vanhoucke, V. Vasudevan, F. Viegas, O. Vinyals, P. Warden, M. Wattenberg, M. Wicke, Y. Yu, X. Zheng, TensorFlow: Large-Scale Machine Learning on Heterogeneous Distributed Systems, 2016.

[43] T. Chen, C. Guestrin, XGBoost: a scalable tree boosting system, in: Proc. 22nd ACM SIGKDD Int. Conf. Knowl. Discov. Data Min, Association for Computing Machinery,

New York, NY, USA, 2016, pp. 785–794, https://doi.org/10.1145/2939672.2939785.
[44] K.T. Schütt, P. Kessel, M. Gastegger, K.A. Nicoli, A. Tkatchenko, K.-R. Müller, SchNetPack: a deep learning toolbox for atomistic systems, J. Chem. Theory Comput. 15 (2019) 448–455, https://doi.org/10.1021/acs.jctc.8b00908.
[45] M.A. Husain, H. Ishqi, S. Rehman, T. Sarwar, S. Afrin, Y. Rahman, Elucidating the interaction of sulindac with calf thymus DNA: biophysical and: in silico molecular modelling approach, New J. Chem. 41 (2017), https://doi.org/10.1039/C7NJ03698A.
[46] M. Bahun, M. Jukić, D. Oblak, L. Kranjc, G. Bajc, M. Butala, K. Bozovičar, T. Bratkovič, Č. Podlipnik, N. Poklar Ulrih, Inhibition of the SARS-CoV-2 3CLpro main protease by plant polyphenols, Food Chem. 373 (2022), 131594, https://doi.org/10.1016/j.foodchem.2021.131594.
[47] B. Ma, X. Li, Resveratrol extracted from Chinese herbal medicines: a novel therapeutic strategy for lung diseases, Chinese Herb. Med. 12 (2020) 349–358, https://doi.org/10.1016/j.chmed.2020.07.003.
[48] H.M. Wahedi, S. Ahmad, S.W. Abbasi, Stilbene-based natural compounds as promising drug candidates against COVID-19, J. Biomol. Struct. Dyn. 39 (2021) 3225–3234, https://doi.org/10.1080/07391102.2020.1762743.
[49] S.H. Manjunath, R.K. Thimmulappa, Antiviral, immunomodulatory, and anticoagulant effects of quercetin and its derivatives: potential role in prevention and management of COVID-19, J. Pharm. Anal. (2021), https://doi.org/10.1016/j.jpha.2021.09.009.
[50] O. Abian, D. Ortega-Alarcon, A. Jimenez-Alesanco, L. Ceballos-Laita, S. Vega, H. T. Reyburn, B. Rizzuti, A. Velazquez-Campoy, Structural stability of SARS-CoV-2 3CLpro and identification of quercetin as an inhibitor by experimental screening, Int. J. Biol. Macromol. 164 (2020) 1693–1703, https://doi.org/10.1016/j.ijbiomac.2020.07.235.
[51] B. Pan, S. Fang, J. Zhang, Y. Pan, H. Liu, Y. Wang, M. Li, L. Liu, Chinese herbal compounds against SARS-CoV-2: Puerarin and quercetin impair the binding of viral S-protein to ACE2 receptor, Comput. Struct, Biotechnol. J. 18 (2020) 3518–3527, https://doi.org/10.1016/j.csbj.2020.11.010.
[52] M. Shohan, R. Nashibi, M.-R. Mahmoudian-Sani, F. Abolnezhadian, M. Ghafourian, S.M. Alavi, A. Sharhani, A. Khodadadi, The therapeutic efficacy of quercetin in combination with antiviral drugs in hospitalized COVID-19 patients: a randomized controlled trial, Eur. J. Pharmacol. 914 (2022), 174615, https://doi.org/10.1016/j.ejphar.2021.174615.
[53] S. Mhatre, N. Gurav, M. Shah, V. Patravale, Entry-inhibitory role of catechins against SARS-CoV-2 and its UK variant, Comput. Biol. Med. 135 (2021), 104560, https://doi.org/10.1016/j.compbiomed.2021.104560.